Microsc. Microanal. Page 1 of 7
doi:10.1017/S1431927611000262

Microscopy AND Microanalysis

Restoration of Uneven Illumination in Light Sheet Microscopy Images

Mohammad Shorif Uddin,[1,†] Hwee Kuan Lee,[1,*] Stephan Preibisch,[2] and Pavel Tomancak[2]

[1]*Imaging Informatics Division, Bioinformatics Institute, 30 Biopolis Street, Singapore 13867*
[2]*Max Planck Institute of Molecular Cell Biology and Genetics, Dresden, Germany*

Abstract: Light microscopy images suffer from poor contrast due to light absorption and scattering by the media. The resulting decay in contrast varies exponentially across the image along the incident light path. Classical space invariant deconvolution approaches, while very effective in deblurring, are not designed for the restoration of uneven illumination in microscopy images. In this article, we present a modified radiative transfer theory approach to solve the contrast degradation problem of light sheet microscopy (LSM) images. We confirmed the effectiveness of our approach through simulation as well as real LSM images.

Key words: digital image processing, image reconstruction-restoration, microscopy, mathematical methods in physics

Introduction

Light microscopy (Murphy & Tanke, 1987; Ploem & Tanke, 2001; Sarder & Nehorai, 2006; Greger et al., 2007; Verveer et al., 2007) images degrade and produce uneven illumination as the incident light is exponentially attenuated along the light path by the distributions of particles in the media. The background media and the overlaps in fluorescence absorption and emission spectra cause multiple scattering of light. This uneven illumination of microscopy image restricts the quantitative analysis of specimen (Van der Kempen et al., 1997). Deconvolution (Agard, 1984; Brakenhoff et al., 1988; Shaw, 1994; Kundur & Hatzinakos, 1996; Sarder & Nehorai, 2006) is a widely used conventional technique to overcome the degradations created by the point spread function (PSF) of microscopes. Although the problem is often ill-posed (Tikhonov & Arsenin, 1977), techniques have been developed to circumvent it. Many deconvolution algorithms can very effectively undo blurring in images that are uniformly blurred. However, the images we set out to restore are not uniformly blurred and therefore making the standard deconvolution algorithms unsuitable for our application.

Besides deconvolution-based restoration, model-based image restoration (Geman & Geman, 1984; Rudin et al., 1992; Combettes & Pesquet, 2004) is also an active area of research. Mathematical models are usually developed based on heuristics or the perception of what an ideal image should be. Such heuristics may originate from prior knowledge of the image. To the best of our knowledge, no known model-based methods are developed to effectively solve uneven illumination due to light attenuation in microscopy.

Recently, there has been an increased interest in the vision research community on image restoration in bad weather conditions based on the physics of attenuation and scattering of light. This method inverts the image formation process to recover a good visibility image of the object, which seems a better choice as it does not require estimating the PSF of the imaging system.

Oakley and Satherley (1998) and Tan and Oakley (2000, 2001) described a physics-based method to restore degraded outdoor scene contrast assuming that scene depths are known beforehand and with the distribution of radiance in the scene by a single Gaussian with known variance. Schechner and Karpel (2004) also used a physical model for image degradation based on scene depth using a couple of images taken through a polarizer at different orientations. Narasimhan and Nayar (2000, 2001, 2002, 2003*a*, 2003*b*) achieved image restoration using a physics-based model describing the scene appearance in uniform bad weather that requires two images of the same scene taken under different weather conditions to compute the scene-depth structure.

Adiga and Chaudhuri (2001) showed some simple methods to correct confocal images for easy interpretation. We have recently deveoped a field theoretical restoration method for confocal microscopy (Lee et al., 2009). In this article, we re-derived our field equations for the restoration of the contrast of light sheet microscopy (LSM) images (Huisken et al., 2004; Keller et al., 2006; Greger et al., 2007; Verveer et al., 2007; Ritter et al., 2008). Though our work is closely related to the works of Narasimhan and Nayar, Oakley and Satherley, Tan and Oakley, and Schechner and Karpel, our technique is greatly different from their methods.

First, they assume a uniform attenuating media, while we extend their formulations for nonuniform attenuation media. Second, the objective of their methods is to calculate the reflectance of objects beyond the attenuation media. Here, we estimate the fluorescence of fluorophores embedded throughout the three-dimensional (3D) volume of the observation space. Finally, they applied their formulation on images of natural scenery that were degraded by bad weather, while we are interested in restoration of images from light microscopy.

Received November 4, 2010; accepted February 21, 2011
**Corresponding author*. E-mail: leehk@bii.a-star.edu.sg
†Current address: Department of Computer Science and Engineering, Jahangirnagar University, Savar, Dhaka 1342, Bangladesh

Physical model

Our model is based on the radiative transfer theory (Chandrasekhar, 1960; Sharkov, 2003). Following Sharkov's formulation, the radiative transfer equation consists of several components at every point in the image. The radiative transfer equation is in general difficult to solve. Our attempt to solve it involves simplifications through *a priori* knowledge of the LSM system. The following is a list of components in the radiative transfer equation (Sharkov, 2003, equation 9.18) and comments on how we handle them in this article.

1. The radiation energy increment due to thermal radiation of the medium: we ignore this term because the laser power in the LSM is comparatively low, and contribution of blackbody radiation at the wavelength of the LSM laser is very small.
2. The radiation energy loss caused by radiation absorption by the medium: this is an important term in our formulation because fluorscence proteins absorb significant amounts of incident laser.
3. The radiation energy increment due to radiation from all directions in the medium: this is the second most important term. It will be shown later that this term contributes ~1% of the image distortion effect.
4. Beam energy loss due to scattering: we ignore this term. Scattering by complex fluorescence proteins is intricate. Furthermore, each pixel element in the image consists of many fluorescence proteins so that we only see the average scattering effects. This term cannot be calculated without going into the details of microscopic interactions of light with proteins.

In summary, we ignore blackbody radiation as it is physically insignificant and a complex scattering phenomena. We based our calculations on radiative loss due to absorption and radiative increment due to radiation from all directions. Finally, we write our radiative transfer equation in a form that is easily applicable and solve for the LSM system. Our equation also includes a term for radiation falling on the camera.

In the subsequent subsections, we present mathematical formulations adapted to LSM (refer to Lee et al., 2009 for a more general formulation). In our model, it is reasonable to assume that the disturbances from the imaging system (water, agarose, etc.) are minor influences compared to light radiation absorption and emission.

Radiative Absorption

Light intensity generally indicates the number of photons passes through a specimen per unit area per unit time. The radiation absorption depends on specimen's property (opaque or transparent) as well as distance traveled through the specimen. Let n_0 be the initial intensity (number of photons per unit area per unit time) that is incident on a specimen. In microscopy, n_0 reflects the incident laser power. Suppose light is incident along the x-axis at a point $\mathbf{r}$. If n number of photons comes out from the specimen, then the number of photons absorbed by the specimen will be $(n - n_0)$. Let $\rho(\mathbf{r})$ be the absorption rate of light per unit length along the path of light at a point $\mathbf{r}$. Then $\rho(\mathbf{r})dl$ will be the probability of light absorbed by the specimen at a point $\mathbf{r}$. With $\rho(\mathbf{r})$ being the probability density of light absorbed by the specimen at a point $\mathbf{r}$, $\rho(\mathbf{r})$ will be high if there are more fluorescent proteins in the specimen. Hence, $\rho(\mathbf{r})$ is proportional to the concentration of proteins at $\mathbf{r}$. Therefore, the final goal of microscopy imaging is to estimate $\rho(\mathbf{r})$, the expected absorption, which is given by

$$dn(\mathbf{r}) = -n(\mathbf{r})\rho(\mathbf{r})dl. \tag{1}$$

Integrating equation (1) gives the light attenuated at a distance l from the initial point,

$$n_A(\mathbf{r}) = n(\mathbf{r}_0)\exp\left(-\int_{\gamma(\mathbf{r}_0:\mathbf{r})}\rho(\mathbf{r})\,dl\right), \tag{2}$$

where the subscript A is the radiation absorption component, r_0 is the initial point along the path of light, $n(\mathbf{r}_0) = n_0$, and $\gamma(\mathbf{r}_0{:}\mathbf{r})$ is a straight line from $\mathbf{r}_0$ to $\mathbf{r}$.

Radiation Emission

Due to overlapping of absorption and emission spectra (Zimmermann et al., 2002) for common fluorophores such as green and yellow fluorescent proteins, the radiation emission from excited fluorophores can be reabsorbed by neighboring fluorophores.

The total incident light flux at a point $\mathbf{r}$ due to radiation falling on $\mathbf{r}$ from all other points in the image will be

$$n_E(\mathbf{r}) = \frac{1}{4\pi}\int_{\mathbf{r}\neq\mathbf{r}'}\frac{n(\mathbf{r}')\rho(\mathbf{r}')\exp\left(-\int_{\gamma(\mathbf{r}':\mathbf{r})}\rho(\mathbf{r}')\,dl\right)}{\|\mathbf{r}-\mathbf{r}'\|^2}\,d\mathbf{r}', \tag{3}$$

where the subscript E is the radiation emission component, and $\gamma(\mathbf{r}'{:}\mathbf{r})$ is a straight line from $\mathbf{r}'$ to $\mathbf{r}$. The inverse square law in the denominator reflects the geometry of 3D space. The term $n(\mathbf{r}')\rho(\mathbf{r}')$ in the numerator gives the total amount of light scattered from $\mathbf{r}'$, and the term $\exp(-\int_{\gamma(\mathbf{r}':\mathbf{r})}\rho(\mathbf{r}')\,dl)$ represents the attenuation of light from $\mathbf{r}'$ to $\mathbf{r}$.

Total Light Flux

We can write the total light flux at a point $\mathbf{r}$ as the sum of absorption and emission components.

$$\begin{aligned} n(\mathbf{r}) &= n_A(\mathbf{r}) + n_E(\mathbf{r}) \\ &= n_0\exp\left(-\int_{\gamma(\mathbf{r}_0:\mathbf{r})}\rho(\mathbf{r})\,dl\right) \\ &\quad + \frac{1}{4\pi}\int_{\mathbf{r}\neq\mathbf{r}'}\frac{n(\mathbf{r}')\rho(\mathbf{r}')\exp\left(-\int_{\gamma(\mathbf{r}':\mathbf{r})}\rho(\mathbf{r}')\,dl\right)}{\|\mathbf{r}-\mathbf{r}'\|^2}\,d\mathbf{r}'. \end{aligned} \tag{4}$$

Discretizing the total light flux equation (4) at point $\mathbf{r}_i$, we have

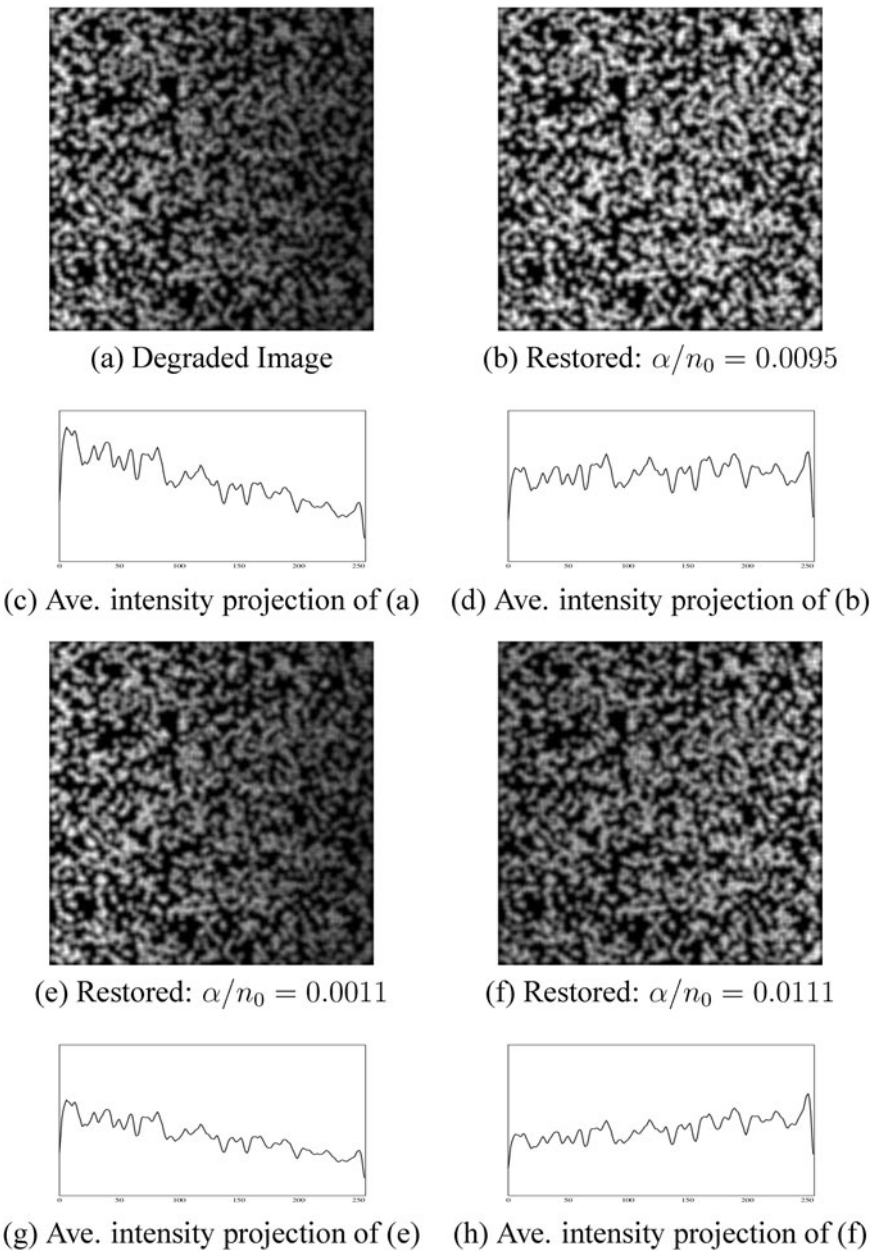

Figure 1. Restoration of a synthetically degraded image: (**a**) shows the degraded image of nonuniform illumination with maximum intensity projection (**c**) falling off exponentially (assuming the light source comes from the left). The parameter $\alpha/n_0 = 0.0095$ gives the best restoration (**b**) in which the maximum intensity projection (**d**) is flat. For small α/n_0, the image is hardly restored (**e**) and for large α/n_0, there is overcompensation of the attenuation effect (**f**). (**g**,**h**) The maximum intensity projection graphs for panels **e** and **f**, respectively. Maximum intensity projection of the degraded image plotted in dashed lines for comparison.

$$n(\mathbf{r}_i) = n_0 \exp\left(-\sum_{k=0}^{i} \rho(\mathbf{r}_k)\Delta x\right) + \frac{1}{4\pi} \sum_{i \neq j} \frac{n(\mathbf{r}_j)\rho(\mathbf{r}_j)\exp\left(-\int \rho(l)\, dl_{ij}\right)}{\|\mathbf{r}_i - \mathbf{r}_j\|^2} \Delta V, \quad (5)$$

where Δx is the interpoint displacement in x-direction between two consecutive points, dl_{ij} is the discretize (infinitesimal) length on the line from point $\mathbf{r}_j$ to point $\mathbf{r}_i$, and ΔV is the infinitesimal volume. Equation (5) can be written as

$$n_0 \exp\left(-\sum_{k=0}^{i} \rho(\mathbf{r}_k)\Delta x\right) = \rho(\mathbf{r}_i) n(\mathbf{r}_i) G(\mathbf{r}_i, \mathbf{r}_j)\big|_{i=j} + \sum_{i \neq j} \rho(\mathbf{r}_j) n(\mathbf{r}_j) G(\mathbf{r}_i, \mathbf{r}_j) = \sum_{\mathbf{r}_j} G(\mathbf{r}_i, \mathbf{r}_j) n(\mathbf{r}_j) \rho(\mathbf{r}_j), \quad (6)$$

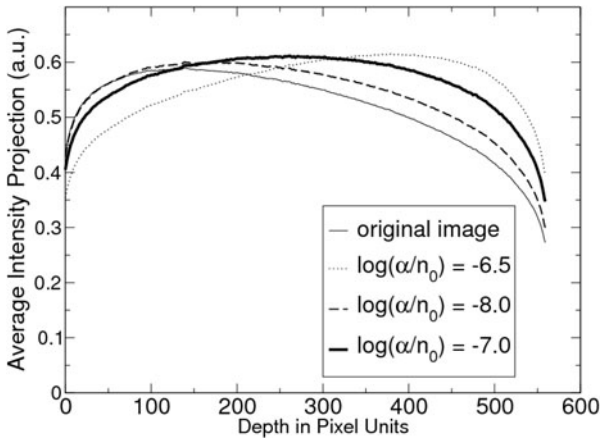

Figure 2. The effectiveness of our method applied to a controlled experiment of uniformly stained round plastic tube is shown. The plot of intensity profile versus depth of the image (thin line) decreases with depth. Although the sample is uniformly stained, a decrease in the intensity profile is due to light attenuation and scattering. Restoration to a uniform illumination is achieved by tunning the free parameter $\log(\alpha/n_0)$ to -7.0. Other values of this parameter either undercompensate (dashed line) or overcompensate (dotted line). Curvature of the intensity profile plot reflects the edge effect of the round plastic tube.

where

$$G(\mathbf{r}_i, \mathbf{r}_j) = \begin{cases} -\dfrac{1}{4\pi} \dfrac{\Delta V \exp\left(-\int \rho(l)\, dl_{ij}\right)}{\|\mathbf{r}_i - \mathbf{r}_j\|^2} & i \neq j \\ \dfrac{1}{\rho(\mathbf{r}_i)} & i = j. \end{cases} \tag{7}$$

Let $u(\mathbf{r}) = n(\mathbf{r})\rho(\mathbf{r})$, which is the absorbed light and is proportional to the observed image intensity. Let $u_0(\mathbf{r})$ be the observed image intensity at $\mathbf{r}$ and α, $(\alpha > 1)$ be a geometrical factor. Physically, α is the ratio between amount of absorbed light by the specimen and amount of emitted light collected by the charge-coupled device (CCD camera). Hence, $u(\mathbf{r}) = \alpha u_0(\mathbf{r})$. If we make a change of variable $u(\mathbf{r}) = n(\mathbf{r})\rho(\mathbf{r})$, then equation (6) becomes

$$n_0 \exp\left(-\sum_{k=0}^{i} \rho(\mathbf{r}_k)\Delta x\right) = \alpha \sum_{\mathbf{r}_j} G(\mathbf{r}_i, \mathbf{r}_j)\, u_0(\mathbf{r}_j). \tag{8}$$

The above equation can be written in matrix form,

$$b = \left(\frac{\alpha}{n_0}\right) G \cdot u_0, \tag{9}$$

$b_i = \exp(-\sum_{k=0}^{i} \rho(\mathbf{r}_k)\Delta x)$ is the attenuation component of light flux, $u_{0i} = u_0(\mathbf{r}_i)$, and G is the matrix defined in equation (7).

Restoration Algorithm

To compute ρ from equation (9), we arrive at the following energy functional,

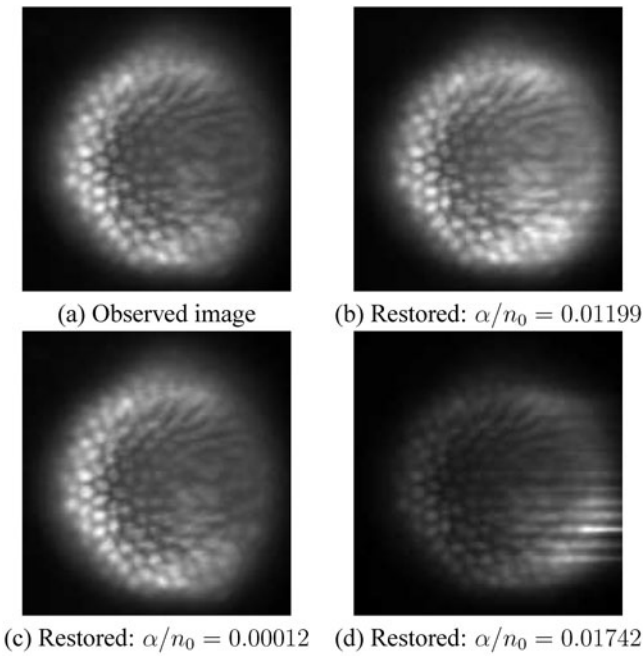

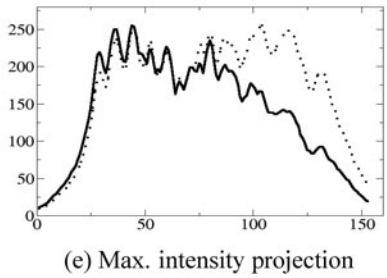

Figure 3. Effect of α/n_0 in the restoration of image due to the attenuation component only: (**a**) the observed image, (**b**) the restored image with the optimum α/n_0 $(= 0.01199)$, (**c**) the restored image with low α/n_0 $(= 0.00012)$, and (**d**) the restored image with high α/n_0 $(= 0.01742)$. (**e**) The maximum intensity profiles for the observed (solid line) and optimum restored (dotted-line) images.

$$J(\rho) = \left\| \mathbf{b}(|\boldsymbol{\rho}|) - \frac{\alpha}{n_0} G(|\boldsymbol{\rho}|) \cdot \mathbf{u}_0 \right\|^2. \tag{10}$$

Note that $J(\rho) \geq 0$ and $J(\rho) = 0$ if and only if equation (9) holds. Hence, the optimized solution of the energy functional gives the best estimate of $\rho(\mathbf{r})$:

$$\boldsymbol{\rho}^* = \left| \arg\min_{\boldsymbol{\rho}} J(\rho) \right|. \tag{11}$$

Absolute values of $\rho(\mathbf{r})$ are used because $\rho(\mathbf{r}) > 0$ by the physical constraint.

Attenuation Only Approximation

If we assume $n_E \ll n_A$, then an analytic solution of equation (10) can be obtained. In this case,

$$G_{(ij)} = \begin{cases} 0 & i \neq j \\ \dfrac{1}{\rho(\mathbf{r_i})} & i = j \end{cases} \tag{12}$$

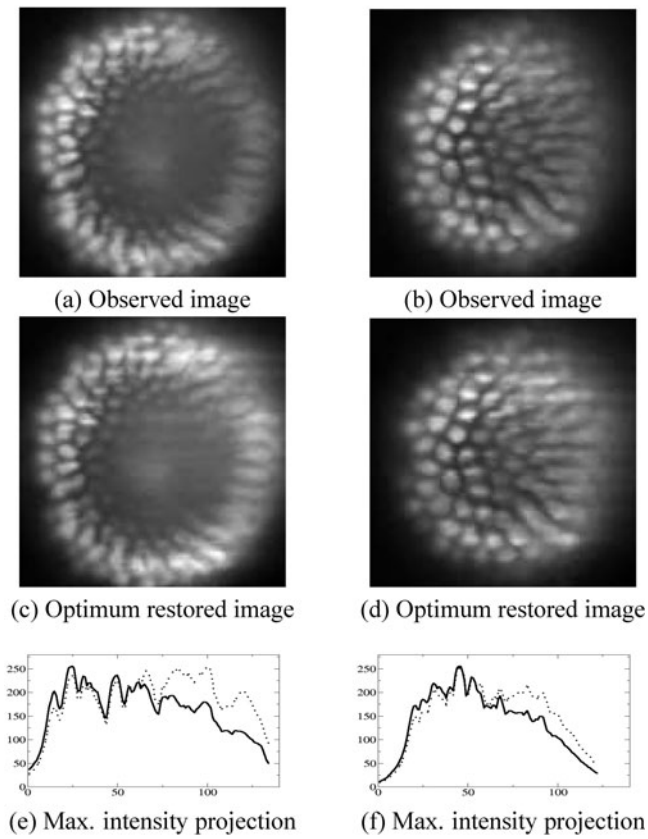

Figure 4. Restoration of two LSM images using the attenuation component only: (**a**) an observed image and its restored view. In panel **e** we plotted the maximum intensity profiles of this observed (solid line) image and its optimum restored (dotted-line) image. (**b**, **d**, **f**) Similar results for another image. In both cases, the intensities of the right part of the restored images are enhanced.

and the solution to equation (10) is

$$\boldsymbol{\rho}_{\mathbf{i}}^{\mathbf{A}} = \frac{\alpha}{n_0}\, u_{0_i} \exp\left(\sum_{k \in \gamma(i0:i)} \rho_k \Delta l_k \right). \tag{13}$$

Minimization of the Energy Functional

Using the estimated $\rho(\mathbf{r})$ from radiation absorption only approximation given by equation (13), we performed the gradient descend method on the objective function $J(\rho)$. For the gradient descend method, we performed the golden section minimization (Kiefer, 1953) on one-dimensional (1D) space in the direction of the steepest gradient descent $dJ/d\rho$. The algorithm is given by:

1. Set initial values of $\rho(\mathbf{r}) = \rho_i^A(\mathbf{r})$.
2. Calculate the direction of steepest descent $dJ/d\rho$.
3. Perform 1D golden section minimization (Kiefer, 1953) in the direction of steepest descent.
4. Iterate steps 2 and 3 until the objective function converged.

Experimental Results and Discussions

Radiation absorption resulted in an unevenly illuminated image. The side of the image nearest to the incident laser appears bright, and the side furthest away appears dark.

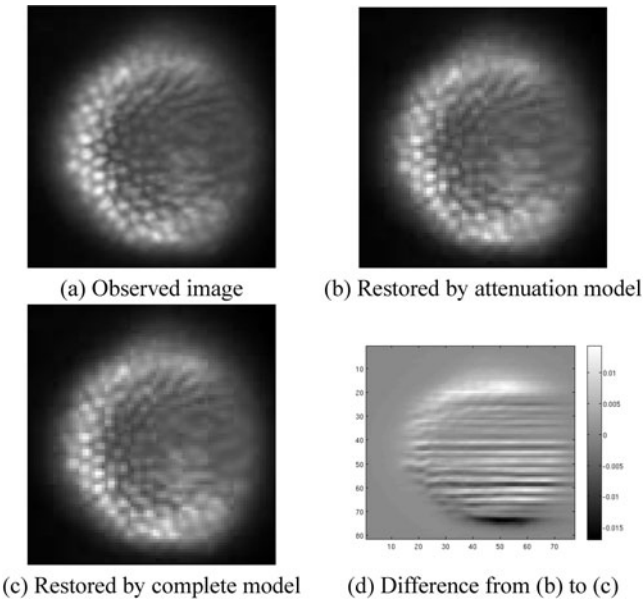

Figure 5. Restoration using the complete physical model: (**a**) the original single plane illumination microscopy image, (**b**) the restored image by the attenuation model, and (**c**) the restored image by using the complete (attenuation + scattering) model. (**d**) The difference image between restored images by the attenuation model and complete model. The horizontal stripes (artifacts) seen in the difference image were removed by the complete model.

Hence the contrast on the dark side becomes poorer as the signal-to-noise ratio decreases. Scattering of light introduces the blurring effect thus reducing resolution. Since we do not model light scattering, our method solves the uneven illumination problem but does not solve the problem of blurring.

Validation and Calibration

Computer Simulation

We performed a computer simulation using synthetically degraded images. The synthetic image with nonuniform illumination (maximum intensity projection falling off exponentially assuming light source comes from the left) was generated from an image of uniform illumination. Figure 1 shows restoration results for a 256 × 256 pixels synthetic image. Here we use equation (13) to restore the image. The tuning parameter α/n_0 can be adjusted to obtain optimal results. n_0 is the incident light intensity, and α is a geometric factor that is usually unknown. For small α/n_0, the image is hardly restored, and for large α/n_0, there is overcompensation of the attenuation effect. The optimal value of α/n_0 is 0.0095 for this image in which the restored image is almost perfectly (uniformly) illuminated.

Controlled Experiment

We performed a controlled experiment to validate and calibrate our model. Alexa-568 fluorophore is dissolved in 1% low melting point agarose and pulled into a small round plastic tube with almost the same refractive index as water (1.333) to prevent the elution of the flurophore. The plastic tube containing the stained agarose is then imaged in the

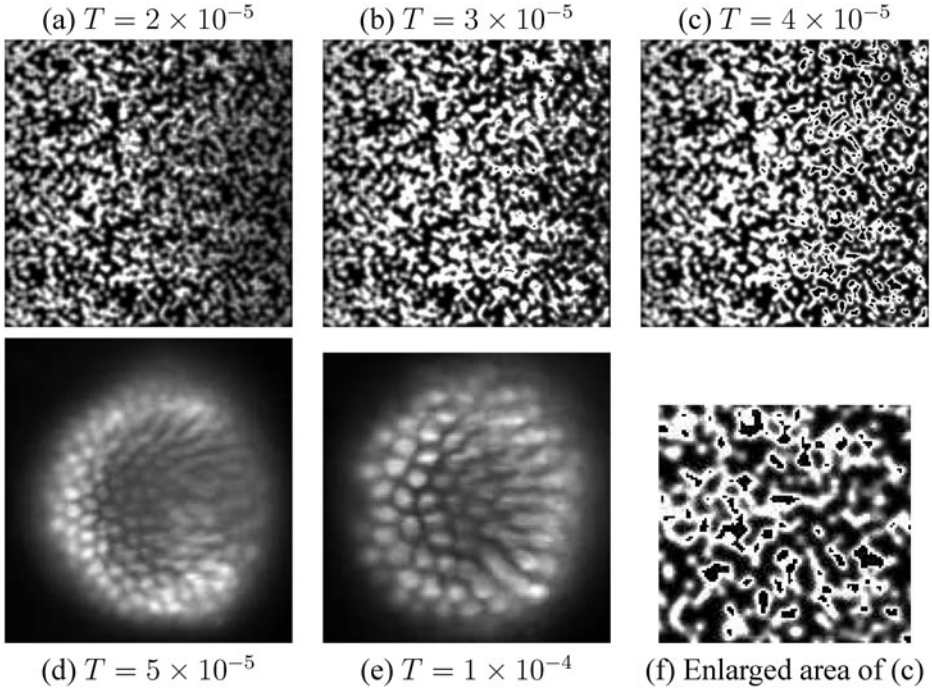

Figure 6. Comparison with the method of Guan et al. (2008). The tuning parameter in their method is a threshold value *T*. Various values of *T* are used to restore the synthetic image of Figure 2. The values of *T* are either (**a**, **b**) too small to compensate for attenuation or (**c**, **f**) too big and overcompensate with artifacts. Restoration of panels **d** and **e** looks fine although under- and overcompensation and artifacts may not be apparent in these images.

water-filled microscope chamber. The purpose of the fluorescent agarose gel in the plastic tube is to provide a uniform fluorescent sample. The diameter of the plastic tube is 1.6 mm with a wall thickness of 0.4 mm and an inner diameter of 0.8 mm. By experimental design, we know that the restored image has to be uniformly illuminated. The image acquired, however, does not show uniform illumination due to light attenuation. We use our model to restore the image to obtain a uniformly illuminated image by adjusting the free parameter α/n_0 in our model. Figure 2 shows the effect of α/n_0 on the restoration model. This parameter is generally unknown but can be calibrated using this method. Note that the curvature of the intensity versus depth plot (Fig. 2) reflects the edge effect of the round plastic tube. Since the sample is uniformly stained, we plot the average intensity project versus depth to average out the noise.

Application to Real Single Plane Illumination Microscopy Images

We applied our physics-based model in the restoration of Drosophila embryo images acquired by LSM (Huisken et al., 2004; Keller et al., 2006; Greger et al., 2007; Verveer et al., 2007; Ritter et al., 2008). The images are rotated in a way so that the laser light is incident on the specimen from left to right in the horizontal direction. The left part of the observed images are bright and clear; however, the right part is darker. Hence, our restoration approach should handle this darker part to make it bright and clear.

At first, we applied our restoration model with only the attenuation component. Figure 3 shows the effect of α/n_0 in the restoration of the image. With low α/n_0 there is no improvement in the restoration, and with high α/n_0 the intensity is overattenuated producing darker image. However, an intermediate α/n_0 between the above two extremes gives optimum restoration. We determined this intermediate optimum α/n_0 from the plot of ρ_{max} versus $\ln(\alpha/n_0)$ plotting. We have also shown the maximum intensity profiles of the observed and optimum restored images for intensity enhancement comparison. From these graphs we see that the intensity of the left part of the restored image is almost the same as that of the observed image; however, the intensity of the right part of the restored image is enhanced.

Similar results are shown in Figure 4. Maximum intensity profiles of the observed and optimum restored images show that the intensities of the left part of the restored images are almost same as that of the observed image; however, the intensities of the right part of the restored images are enhanced.

Now we used our complete physical model (considering both absorption and emission phenomena) for restoration. Figure 5 shows an improvement in restoration using the complete model compared to the attenuation component only. This improvement is due to the removal of artifacts (tiny horizontal stripes, approximately 1%) caused by the compensation of light attenuation.

We also compare our results with an adaptive correction technique for 3D reconstruction of microscopy images (Guan et al., 2008). This method was developed for 3D images; however, we rederive the equations and adapt it to LSM images. The tuning parameter for this method is a

threshold value T. Higher T values resulted in more intensity compensation and vice versa. Figure 6 shows the restoration of the synthetic image from Figure 1. We tried a wide range of tuning parameters but could not obtain uniformly illuminated restored images. Figure 6a is clearly undercompensated. Figure 6b looks undercompensated on the right side and small artifacts start to appear. At higher values of T (Fig. 6c), we observed artifacts (Fig. 6f). Restoration for Drosophila embryo images looks fine. However, the ground truth of these images is unknown, and nonuniformity of illumination may not be obvious in these complex images.

Conclusions

In this article, we addressed the problem of uneven (space variant) contrast restoration of microscopy images by proposing a physics-based model of light absorption and emission. The entire mathematical formulation is presented for LSM. Our technique efficiently restored the unevenly illuminated images on synthetically degraded images and a controlled experiment using a uniformly fluorescent sample, which can be used to calibrate the method. The application of our technique to the restoration of real LSM images of Drosophila efficiently restored unevenly illuminated images.

References

Adiga, P.S.U. & Chaudhuri, B.B. (2001). Some efficient methods to correct confocal images for easy interpretation. *Micron* **32**, 363–370.

Agard, D.A. (1984). Optical sectioning microscopy: Cellular architecture in three dimensions. *Ann Rev Biophys Bioeng* **13**, 191–219.

Brakenhoff, G., Van der Voort, H.T., Van Spronson, E.A. & Nanninga, N. (1988). 3-dimensional imaging of biological structures by high resolution confocal scanning laser microscopy. *Scanning Microscopy* **2**, 33–40.

Chandrasekhar, S. (1960). *Radiative Transfer*, Chesapeake, VA: Dove Publications.

Combettes, P.L. & Pesquet, J.C. (2004). Image restoration subject to a total variation constraint. *IEEE T Image Process* **13**, 1213–1222.

Geman, S. & Geman, G. (1984). Stochastic relaxation, Gibbs distributions, and the Bayesian restoration of images. *IEEE T Pattern Anal* **6**, 721–741.

Greger, K., Swoger, J. & Stelzer, E.H.K. (2007). Basic building units and properties of a fluorescence single plane illumination microscope. *Rev Sci Instrum* **78**, 023705.

Guan, Y.Q., Cai, Y.Y., Zhang, X., Lee, X.Y. & Opas, M. (2008). Adaptive correction technique for 3D reconstruction of fluorescence microscopy images. *Microsc Res Techniq* **71**, 146–157.

Huisken, J., Swoger, J.J., Del Bene, F., Wittbrodt, J. & Stelzer, E.H.K. (2004). Optical sectioning deep inside live embryos by selective plane illumination microscopy. *Science* **305**, 1007–1009.

Keller, P.J., Pampaloni, F. & Stelzer, E.H.K. (2006). Life sciences require the third dimension. *Curr Opin Cell Biol* **18**, 117–124.

Kiefer, J. (1953). Sequential minimax search for a maximum. *Proc Amer Math Soc* **4**(3), 502–506.

Kundur, D. & Hatzinakos, D. (1996). Blind image deconvolution. *IEEE Signal Proc Mag* **13**, 43–64.

Lee, H.K., Uddin, M.S., Sankaran, S., Hariharan, S. & Ahmed, S. (2009). A field theoretical restoration methdod for images degraded by non-uniform light attenuation: An application for light microscopy. *Opt Express* **17**, 11294–11308.

Murphy, D.B. & Tanke, H.J. (1987). *Fundamentals of Light Microscopy and Electronic Imaging*. New York: Oxford University Press.

Narasimhan, S.G. & Nayar, S.K. (2000). Chromatic framework for vision in bad weather. *Proceedings of International Conference on Computer Vision and Pattern Recognition*, Hilton Head, SC, June 2000, pp. 598–605.

Narasimhan, S.G. & Nayar, S.K. (2001). Removing weather effects from monochrome images. *Proceedings of International Conference on Computer Vision and Pattern Recognition*, Lihue, Hawaii, June 2001, pp. 186–193.

Narasimhan, S.G. & Nayar, S.K. (2002). Vision and the atmosphere. *Int J Computer Vision* **48**, 233–254.

Narasimhan, S.G. & Nayar, S.K. (2003*a*). Contrast restoration of weather degraded images. *IEEE T Pattern Anal* **25**, 713–724.

Narasimhan, S.G. & Nayar, S.K. (2003*b*). Polarization based vision through haze. *Appl Opt* **42**, 511–525.

Oakley, J.P. & Satherley, B.L. (1998). Improving image quality in poor visibility conditions using a physical model for degradation. *IEEE T Image Process* **7**, 167–179.

Ploem, J.S. & Tanke, H.J. (2001). *Introduction to Fluorescence Microscopy*. New York: Wiley Liss, Inc.

Ritter, J.G., Veith, R., Siebrasse, J. & Kubitscheck, U. (2008). High-contrast single-particle tracking by selective focal plane illumination microscopy. *Opt Express* **16**, 7142–7152.

Rudin, L., Osher, S. & Fatemi, E. (1992). Nonlinear total variation based noise removal algorithms. *Physica D* **60**, 259–268.

Sarder, P. & Nehorai, A. (2006). Deconvolution methods for 3-D fluorescence microscopy images. *IEEE Signal Process Mag* **23**, 32–45.

Schechner, Y.Y. & Karpel, N. (2004). Clear underwater vision. *Proceedings of IEEE Conference on Computer Vision and Pattern Recognition*, Washington, DC, pp. 536–543.

Sharkov, E.A. (2003). *Passive Microwave Remote Sensing of the Earth*. Chichester, UK: Praxis Publishing Ltd.

Shaw, P. (1994). Deconvolution in 3-D optical microscopy. *Histochem J* **26**, 1573–6865.

Tan, K. & Oakley, J.P. (2000). Enhancement of color images in poor visibility conditions. *Proceedings of International Conference on Image Processing*, Vancouver, BC, Canada, September 10–13, 2000, pp. 788–791. Washington, DC: IEEE Computer Society.

Tan, K. & Oakley, J.P. (2001). Physics based approach to color image enhancement in poor visibility conditions. *J Opt Soc Am A* **18**, 2460–2467.

Tikhonov, A.N. & Arsenin, V.Y. (1977). *Solutions of Ill-Posed Problems*. New York: Wiley.

Van der Kempen, G.M.P., van Vliet, L.J, Verveer, P.J. & Van der Voort, H.T.M. (1997). A quantitative comparison of image restoration methods for confocal microscopy. *J Microsc* **185**, 354–365.

Verveer, P.J., Swoger, J., Pampaloni, F., Greger, K., Marcello, M. & Stelzer, E.H.K. (2007). High-resolution three dimensional imaging of large specimens with light sheet-based microscopy. *Nat Methods* **4**, 311–313.

Zimmermann, T.J., Rietdorf, J., Girod, T.A., Georget, J. & Pepperkok, R. (2002). Spectral imaging and linear un-mixing enables improved FRET efficiency with a novel GFP2–YFP FRET pair. *FEBS Lett* **531**, 245–249.